



Natural convection heat transfer utilizing nanofluid in a cavity with a periodic side-wall temperature in the presence of a magnetic field

Wisam K. Hussam^{a,b,*}, Khalil Khanafer^a, Hayder J. Salem^a, Gregory J. Sheard^b

^a School of Engineering, Australian College Kuwait, Safat, Kuwait

^b The Sheard Lab, Department of Mechanical and Aerospace Engineering, Monash University, VIC 3800, Australia

ARTICLE INFO

Keywords:

Periodic natural convection
Numerical
Cavity
Magnetohydrodynamics
Nanofluid

ABSTRACT

Natural convection in a square cavity filled with electrically conducting nanofluid that is driven by a periodic temperature profile along one of the vertical walls is studied numerically. The top and bottom horizontal walls are kept adiabatic. The right wall is maintained at low temperature while the temperature of the opposing vertical wall varies sinusoidally with time about a mean temperature. Flow and heat transfer performance through the enclosure is examined over a wide range of oscillation amplitudes and frequencies, Hartmann number, Rayleigh number and solid volume fraction at Prandtl number $Pr = 6.2$. The results show that oscillation amplitude, A , and frequency, f , of the vertical wall significantly affect the response of heat transfer inside the cavity. For $A > 0.5$, the forcing frequency is found to remain almost constant at $f = 2.5$, while it shifts towards a higher frequency $f = 5$ for $A \leq 0.5$. At low Rayleigh number, Nusselt number is found to be independent of Rayleigh and Hartman numbers, while at higher Rayleigh number, convective flow dominates, and Nusselt number becomes independent of Hartmann number. In this regime, the Nusselt scaling with Rayleigh number agrees well with the exponent predicted by theory of natural convection in a cavity without magnetic field or nanoparticles, with a value of $1/4$. With the increase of solid volume fraction, the heat transfer rate may increase or decrease depending on the values of Hartmann and Rayleigh numbers.

1. Introduction

Natural convection flow and heat transfer in enclosures have received considerable attention in the past few decades. This interest stems from its importance in many industrial and engineering applications. Such applications include electronic packaging, cooling of electrical equipment, solar collectors, nuclear reactors and crystals manufacturing [1–10]. The convection of electrically conducting fluid in the presence of a magnetic field has also been studied by many researchers numerically and experimentally [11–17]. In material manufacturing technology, researchers apply an external magnetic field to suppress unavoidable convection currents for superior control of crystal quality. For example, the mechanism of the crystal growth in the presence of magnetic field was examined by Oreper and Szekely [16]. They found that the magnetic field can suppress natural convection and that the strength of the magnetic field is one of the important factors during crystal formation. Alchaar et al. [18] numerically studied two dimensional natural convection in a shallow cavity heated from below in the presence of an inclined magnetic field. Their results demonstrated that the effect of the magnetic field was to reduce heat transfer and inhibit

the onset of the convection current.

Khanafer and Chamkha [18] numerically studied hydromagnetic natural convection from an inclined porous square enclosure with heat generation. The effect of magnetic field was found to suppress natural convection activities within the enclosure. Al-Najem et al. [11] numerically investigated laminar natural convection in a tilted enclosure with a transverse magnetic field. Their results found that the heat transfer mechanisms and the flow characteristics inside the tilted enclosures were shown to depend strongly upon both the strength of the magnetic field and the inclination angle. Furthermore, significant suppression of the convective current was obtained by applying a strong magnetic field. MHD natural convection flow in cavities filled with square solid blocks was studied by Ashouri et al. [19]. The aim of that investigation was to study the influence of magnetic field on natural convection inside enclosures partially filled with conducting square solid obstacles. The results reported by the authors indicated that both the magnetic field and solid blocks can significantly influence the flow and temperature fields.

Nanotechnology has been used extensively in various industrial and biomedical applications. Recent advances in nanotechnology have led

* Corresponding author at: School of Engineering, Australian College Kuwait, Safat, Kuwait
E-mail address: w.alsaadi@ack.edu.kw (W.K. Hussam).

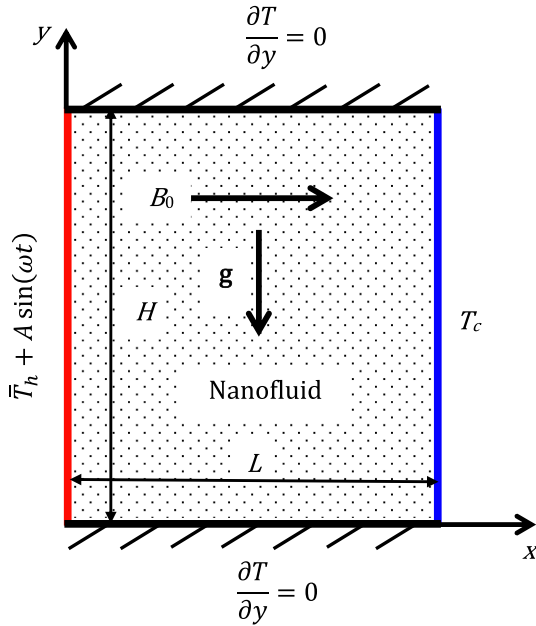


Fig. 1. Schematic diagram of the enclosure geometry with temperature boundary conditions. A square cavity with $H = L$ is considered throughout this study and No-slip conditions ($\mathbf{u} = 0$) is imposed on all boundaries.

kept at a uniform low temperature T_c and the left vertical wall is maintained at a sinusoidal temperature variation in time with an average temperature of \bar{T}_h ($\bar{T}_h > T_c$). The nanofluid is permeated by a uniform external magnetic field (B_0) applied along the x -axis. The resulting convective flow is governed by the combined mechanism of the driving buoyancy force and the electromagnetic braking force. The magnetic Reynolds number Re_m , which represents the ration between the induced and applied magnetic field is assumed to satisfy $Re_m \ll 1$ so that the induced magnetic field produced by the motion of the electrically conducting fluid is negligible compared to the externally applied magnetic field B_0 . The Joule heating of the fluid and the effect of viscous dissipation are also negligible. The thermo-physical properties of the base fluid and the antiparticles are given in Table 1. A Boussinesq approximation for fluid buoyancy is employed, in which density differences in the fluid are neglected except through the gravity term in the momentum equation. Under this approximation the fluid temperature is related linearly to the density via a thermal expansion coefficient α and the energy equation reduces to a scalar advection diffusion equation for temperature which is evolved in conjunction with the velocity field [35,36]. Under these assumption, the conservation equations of mass, momentum and energy for laminar and unsteady-state natural convection in a two-dimensional Cartesian coordinate system can be written as

$$\frac{\partial u}{\partial x} + \frac{\partial v}{\partial y} = 0 \tag{1}$$

$$\frac{\partial u}{\partial t} + u \frac{\partial u}{\partial x} + v \frac{\partial u}{\partial y} = -\frac{1}{\rho_{nf}} \frac{\partial p}{\partial x} + \nu_{nf} \left(\frac{\partial^2 u}{\partial x^2} + \frac{\partial^2 u}{\partial y^2} \right) \tag{2}$$

$$\frac{\partial v}{\partial t} + u \frac{\partial v}{\partial x} + v \frac{\partial v}{\partial y} = -\frac{1}{\rho_{nf}} \frac{\partial p}{\partial y} + \nu_{nf} \left(\frac{\partial^2 v}{\partial x^2} + \frac{\partial^2 v}{\partial y^2} \right) + \frac{1}{\rho_{nf}} (\rho\beta)_{nf} g (T - T_c) - \frac{\sigma_{nf} B^2 v}{\rho_{nf}} \tag{3}$$

$$\frac{\partial T}{\partial t} + u \frac{\partial T}{\partial x} + v \frac{\partial T}{\partial y} = \alpha_{nf} \left(\frac{\partial^2 T}{\partial x^2} + \frac{\partial^2 T}{\partial y^2} \right) \tag{4}$$

The effect of the electromagnetic field is introduced into the momentum equation by the Lorentz force term $\mathbf{J} \times \mathbf{B}$, which represents the vector product of the electric current density and magnetic field. The

Poisson equation for the electrical potential is obtained by combining Ohm's law and the conservation of electric current, respectively written as

$$\mathbf{J} = \sigma (-\nabla\Phi + \mathbf{V} \times \mathbf{B}) \tag{5}$$

$$\nabla \cdot \mathbf{J} = 0 \tag{6}$$

which yields

$$\nabla^2 \Phi = B_0 \left(\frac{\partial U}{\partial Y} - \frac{\partial V}{\partial X} \right) \tag{7}$$

where \mathbf{J} , \mathbf{V} and Φ are the electric current density, velocity vector and electric potential, respectively. As discussed by Pirmohammadi et al. [37], for the case of two-dimensional cavity flow with an electrically insulating boundary ($\sigma = 0$) on which $\partial\Phi/\partial n = 0$, Eq. (7) reduces to $\nabla^2 \Phi = 0$, which means that the electric potential vanishes everywhere in the cavity. Therefore, the Lorentz force reduces to a damping factor $-\sigma B_0^2 v$.

The thermo-physical properties of nanofluids can be determined using the following models as [20,22,38].

$$\rho_{nf} = (1 - \phi)\rho_f + \phi\rho_p \tag{8}$$

$$\sigma_{nf} = (1 - \phi)\sigma_f + \phi\sigma_p \tag{9}$$

$$(\rho C_p)_{nf} = (1 - \phi)(\rho C_p)_f + \phi(\rho C_p)_p \tag{10}$$

$$(\rho\beta)_{nf} = (1 - \phi)(\rho\beta)_f + \phi(\rho\beta)_p \tag{11}$$

$$\alpha_{nf} = \frac{k_{nf}}{(\rho C_p)_f} \tag{12}$$

In these equations, ϕ is the solid volume fraction, σ is the electrical conductivity, ρ is the density, α is the thermal diffusivity, C_p is the specific heat and β is the thermal expansion coefficient of the nanofluid. The effective viscosity of a fluid containing a dilute suspension of small rigid spherical particles is given as [39].

$$\frac{\mu_{nf}}{\mu_f} = \frac{1}{(1 - \phi)^{2.5}} \tag{13}$$

The effective thermal conductivity of the nanofluid, taking into account the effect of a liquid nanolayer on the surface of a nanoparticle is used in this investigation [40].

$$\frac{k_{nf}}{k_f} = \frac{k_p + 2k_f - 2(k_f - k_p)(1 + \eta)^3 \phi}{k_p + 2k_f + (k_f - k_p)(1 + \eta)^3 \phi} \tag{14}$$

where η is the ratio of the nanolayer thickness to the original particle radius. $\eta = 0.1$ is used throughout this study [34].

Introducing the dimensionless parameters,

$$\begin{aligned} \tau &= \frac{\alpha_f t}{L^2}, X = \frac{x}{L}, Y = \frac{y}{L}, U = \frac{uL}{\alpha_f}, V = \frac{vL}{\alpha_f}, \\ \theta &= \frac{T - T_c}{T_h - T_c}, P = \frac{\rho L^2}{\rho_{nf} \alpha_f^2}, Ha = B_0 L \sqrt{\frac{\sigma_{nf}}{\rho_{nf} \nu_f}}, \\ Ra &= \frac{g \beta_f (T_h - T_c) L^3}{\nu_f \alpha_f}, Pr = \frac{\nu_f}{\alpha_f}. \end{aligned} \tag{15}$$

Eqs. (1)–(4) can be converted to non-dimensional form as

Table 1
Thermophysical properties of water and nanoparticles [34].

Physical properties	Water	Cu
ρ (kg/m ³)	997.1	8933
C_p (J/kg.K)	4179	385
k (W/m.K)	0.613	400
$\alpha \times 10^7$ (m ² /s)	1.47	1163.1
$\beta \times 10^6$ (1/K)	210	51

$$\frac{\partial U}{\partial X} + \frac{\partial V}{\partial Y} = 0, \tag{16}$$

$$\frac{\partial U}{\partial \tau} + u \frac{\partial U}{\partial X} + v \frac{\partial U}{\partial Y} = -\frac{\partial P}{\partial X} + \frac{\nu_{nf}}{\alpha_f} \left(\frac{\partial^2 U}{\partial X^2} + \frac{\partial^2 U}{\partial Y^2} \right), \tag{17}$$

$$\frac{\partial V}{\partial \tau} + u \frac{\partial V}{\partial X} + v \frac{\partial V}{\partial Y} = -\frac{\partial p}{\partial Y} + \frac{\nu_{nf}}{\alpha_f} \left(\frac{\partial^2 V}{\partial X^2} + \frac{\partial^2 V}{\partial Y^2} \right) + \frac{(\rho\beta)_{nf}}{\rho_{nf}\beta_f} Ra Pr \theta - Ha^2 Pr V, \tag{18}$$

$$\frac{\partial \theta}{\partial \tau} + u \frac{\partial \theta}{\partial X} + v \frac{\partial \theta}{\partial Y} = \frac{\alpha_{nf}}{\alpha_f} \left(\frac{\partial^2 \theta}{\partial X^2} + \frac{\partial^2 \theta}{\partial Y^2} \right). \tag{19}$$

The non-dimensional initial and boundary conditions used in this investigation are given as

$$\begin{aligned} U = V = 0, \quad \theta = 0 \quad \text{at } \tau = 0, \\ U = V = 0, \quad \theta = 1 + A \sin\left(\frac{2\pi\tau}{\tau_p}\right) \quad \text{at } X = 0, \\ U = V = 0, \quad \theta = 0 \quad \text{at } X = 1, \\ U = V = 0, \quad \frac{\partial \theta}{\partial Y} = 0 \quad \text{at } Y = 0, 1, \end{aligned} \tag{20}$$

where $\tau_p = \alpha_f \tau_p / L^2$ and $f = \omega L^2 / \alpha_f$ are respectively, the dimensionless time period and frequency of the temperature oscillation and the amplitude of the temperature oscillation is non-dimensionalized by $(T_h - T_c)$. The temporal variation of the average Nusselt number along the left high temperature oscillating wall and the right constant cold temperature wall are defined as

$$\bar{Nu}_h = -\int_0^1 \frac{k_{nf}}{k\rho} \frac{\partial \theta}{\partial X} \Big|_{X=0} dY, \tag{21}$$

$$\bar{Nu}_c = -\int_0^1 \frac{k_{nf}}{k\rho} \frac{\partial \theta}{\partial X} \Big|_{X=1} dY. \tag{22}$$

The time-averaged Nusselt number over one time period at hot and cold walls can be defined as

$$\bar{\bar{Nu}}_h = -\frac{1}{\tau_p} \int_0^{\tau_p} \int_0^1 \frac{k_{nf}}{k\rho} \frac{\partial \theta}{\partial X} \Big|_{X=0} dY d\tau, \tag{23}$$

$$\bar{\bar{Nu}}_c = -\frac{1}{\tau_p} \int_0^{\tau_p} \int_0^1 \frac{k_{nf}}{k\rho} \frac{\partial \theta}{\partial X} \Big|_{X=1} dY d\tau. \tag{24}$$

3. Numerical methodology

The governing flow and energy equations associated with the initial and boundary conditions are solved numerically using a higher-order in-house solver, which employs a spectral-element method for spatial discretization and a third-order time integration scheme based on backwards-differencing [41]. The enclosure is discretized with 962 quadrilateral spectral elements in the x - y plane. Care was taken to ensure that the flow was resolved in the vicinity of the walls, particularly the heated boundary, with coarser grid spacing in the interior.

A grid resolution study was undertaken to determine a suitably accurate order for the tensor-product polynomial shape functions within each element. Convergence tests were performed on two cases chosen at the upper end of the parameter range of this study. The first case featured $a = 2$, $Ra = 10^7$, $Ha = 100$, $\tau_p = 0.001$ and $\phi = 0.2$, and the second featured $a = 2$, $Ra = 10^7$, $Ha = 0$, $f = 100$ and $\phi = 0.05$ and 0.2 . The results of these tests are shown in Table 2. It is found that the results are converged to within less than 0.5% with polynomial order $N_p = 6$, which is hereafter used for the simulations reported in this study.

For time integration of eqs. (16–19), the advection/convection terms are concurrently solved explicitly, followed by a projection of the velocity field onto a divergence-free space, and finally implicitly solves for velocity components and temperature. This procedure extends the

backwards differentiation algorithm of Karniadakis et al. [41] to the coupled Boussinesq equations. The temperature transport formulation of the present code has been validated in studies on buoyancy-driven flows [35,36].

To validate the numerical scheme being used, the numerical system was first tested for the case of natural convection in a cavity with time-dependent boundary condition for $Ha = 0$ and $\phi = 0$. Computed average Nusselt numbers \bar{Nu} for heat transfer with $Pr = 7$, $a = 0.2, 0.4, 0.8$, $\tau_p = 0.01$ and $Ra = 1.45 \times 10^5$ were compared against the numerical results of Kazmierczak and Chinoda [33] and Wang et al. [34]. The results of this comparison are presented in Table 3, which compare well with the published data.

In addition, the numerical system was further tested against the study of natural convection with nanofluids in zero- Ha and non-zero- Ha . Computed average Nusselt numbers \bar{Nu} for heat transfer with $Pr = 6.2$, $Ha = 0$ and 30 , $\phi = 0.03, 0.1$ and $Ra = 1 \times 10^5$ were compared against the numerical results of Hammami et al. [42] and Pirmohammadi et al. [37]. The results of this comparison are presented in Table 4, where a pleasing agreement is seen.

4. Results and discussion

To get an oscillating solution independent of the initial conditions, at least 4–8 oscillation periods needed to be computed. Results are computed for a wide range of parameters where the temperature amplitude is varied over the range $0 \leq A \leq 2$, while the forcing frequency is varied $0 \leq f \leq 100$. Hartmann number, Rayleigh number, and the solid void fraction are varied as $0 \leq Ha \leq 100$, $10^3 \leq Ra \leq 10^9$, and $0 \leq \phi \leq 0.2$, respectively. Throughout the computations, a time step size of $\Delta\tau = 10^{-6}$ is used for $Ra \leq 10^7$, while a time step size of $\Delta\tau = 10^{-7}$ is used for $Ra = 10^8$ and $Ra = 10^9$. Thus, for example, 2×10^6 and 1×10^4 time integration steps are needed for $f = 0.5$ and 100 , respectively for $\Delta\tau = 10^{-6}$.

Results are presented in three subsections. Firstly, the effect of oscillation frequency and amplitude on heat transfer for a fixed combination of Ha , Ra and ϕ is reported. This is followed by considering the effect of Hartmann number, Rayleigh number and nanoparticle mass fraction on heat transfer. Finally, temperature and streamline fields in the enclosure are presented.

Fig. 2 shows the variation of time-averaged Nusselt number over a broad range of forcing frequency and for a selection of forcing amplitudes for $Ra = 10^6$, $Ha = 100$ and $\phi = 0.2$. It can be noted that there is a significant enhancement in heat transfer for higher amplitudes where a progressive increase in the peak Nusselt number is generated with increasing the forcing amplitude. It is interesting to observe that as the oscillation amplitude increases, the frequency where the peak Nusselt number occurs, remains almost constant at $f = 2.5$ for $A > 0.5$, and increases to $f = 5$ for $A \leq 0.5$. The response in terms of peak frequency with increasing amplitude was found to be similar to the case of torsionally oscillating cylinder in MHD duct flow [43].

Table 2

Convergence of the average Nusselt number \bar{Nu} with increasing polynomial order for oscillating amplitude $A = 2$, time period $f = 100$, Rayleigh number $Ra = 10^7$ at different Hartman numbers and solid void fractions. A polynomial degree of $N_p = 6$ was chosen for the simulations in the present study.

N_p	\bar{Nu}			
	$Ha = 0$		$Ha = 100$	
	$\phi = 0.05$	$\phi = 0.2$	$\phi = 0.05$	$\phi = 0.2$
4	16.307	17.228	24.586	32.758
5	16.450	17.251	24.621	32.882
6	16.336	17.259	24.689	32.998
7	16.379	17.273	24.763	32.024
8	16.385	17.288	24.793	32.114

Table 3

Comparison of results to published work for for $Ra = 1.4 \times 10^5$, $Pr = 7$ and $\tau_p = 0.01$ at different values of oscillating amplitudes in a zero- Ha and zero- ϕ flow.

a	\overline{Nu}		
	Present study	Kazmierczak [33]	Wang [34]
0.2	5.24	5.35	5.27
0.4	5.29	5.41	5.31
0.8	5.46	5.58	5.48

Table 4

Comparison of results to published work for for $Ra = 1 \times 10^5$ for different Hartmann numbers, solid volume fractions and Prandtl numbers as indicated.

Ha	\overline{Nu}				
	ϕ	Pr	Present study	HHMM [42]	PGS [37]
0	0.03	6.2	4.88	4.86	–
0	0.10	6.2	5.22	5.25	–
30	0.03	6.2	3.03	3.02	–
100	0	0.73	1.35	–	1.37

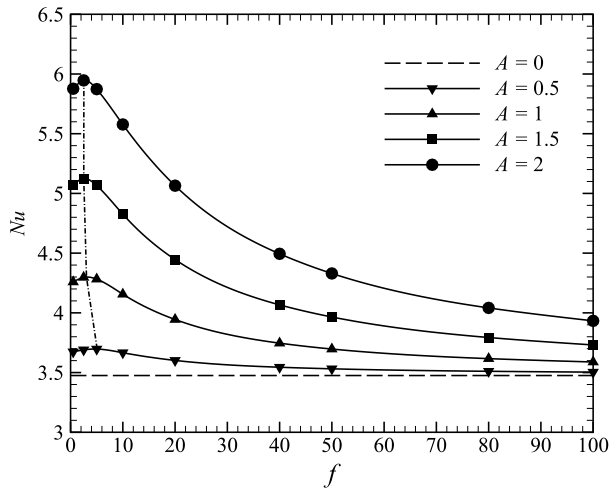


Fig. 2. Time-averaged Nusselt number plotted against temperature oscillation frequency for different oscillation amplitudes for $Ra = 10^6$, $Ha = 100$ and $\phi = 0.2$. For reference, Nusselt number for the case without oscillation is shown by the horizontal dashed line. The dashed-dot-line curve shows the locus of maximum Nusselt number as a function of f .

The sequence of streamline and temperature contours plotted at four different times over the duration of one period for $A = 2$ and $A = 0.5$, and the frequency where the peak Nusselt number occurs (Ref. Fig. 2) are shown in Fig. 3 and Fig. 4, respectively. The contours shown in Figs. 3 and 4, are plotted in equal increments of $1/4\tau_p$. For both amplitudes, the streamlines are dominated by a primary cell rotating in a clockwise direction and filling most of the enclosure. However, the location of ψ_{max} in the cell shifts from the hot side to cold side in a different fashion and with maximum magnitude changes with time at the higher amplitude. A secondary cell was observed at the upper left hand corner (Fig. 4(b)) and the right hand corner (Fig. 4 (d)) of the enclosure at the higher amplitude.

The isotherms plotted in these figures reveal that regardless of the amplitude value, a thermal boundary layer is visible on the hot wall. The hot fluid next to the hot wall rises vertically and replacing the cold fluid that transport horizontally towards the cold wall. The hot buoyant fluid rises to the top of the enclosure and form a warm pocket which contains fluid warmer than the hot wall. However, the warm pocket

near the top wall of the enclosure exists for longer duration for $A = 2$ (Fig. 4(b-c)). This warm region near the top wall vanishes in the next cycle as energy diffuses and is advected outward until finally achieving the rising hot wall temperature.

The dependence of the average Nusselt number on the Rayleigh number at different Hartmann numbers for $A = 2$ and $\phi = 0.2$ is shown in Fig. 5. For a given Hartmann number, the Nusselt number passes through different regimes as Rayleigh number increases. At $Ra = 10^3$, it is found that the flow is diffusion dominated and the Nusselt number is independent of both Rayleigh number and Hartmann number. In this regime, the flow lacks a distinct boundary layer adjacent to the side-wall boundary. At high Rayleigh numbers, convection effects become significant and the Nusselt number start increasing with Rayleigh

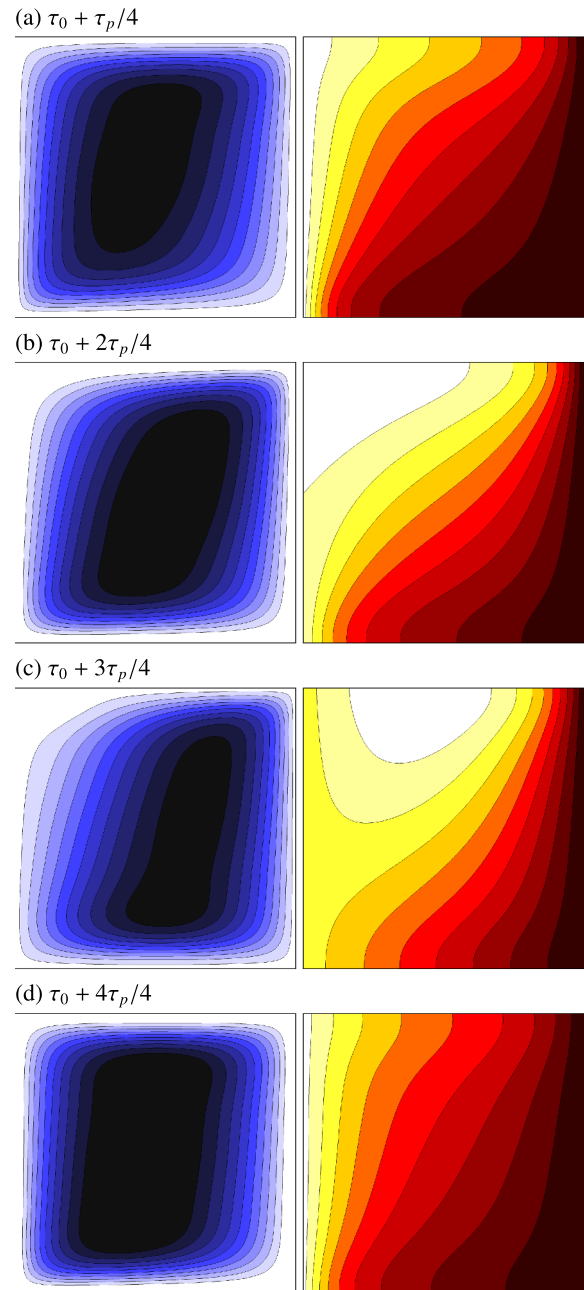


Fig. 3. Contour plots of streamlines (left) and temperature (right) during one period of oscillation for $A = 0.5$, $f = 5$, $\phi = 0.2$, $Ra = 1e6$ and $Ha = 100$. The minimum and maximum levels of ψ and θ , respectively, are (a) 0.5 to 5, (b) 0.5 to 3.5, (c) 0.2 to 2.2 and (d) 0.5 to 3, and (a) 0 to 1.4, (b) 0 to 1, (c) 0 to 0.6 and (d) 0 to 0.95.

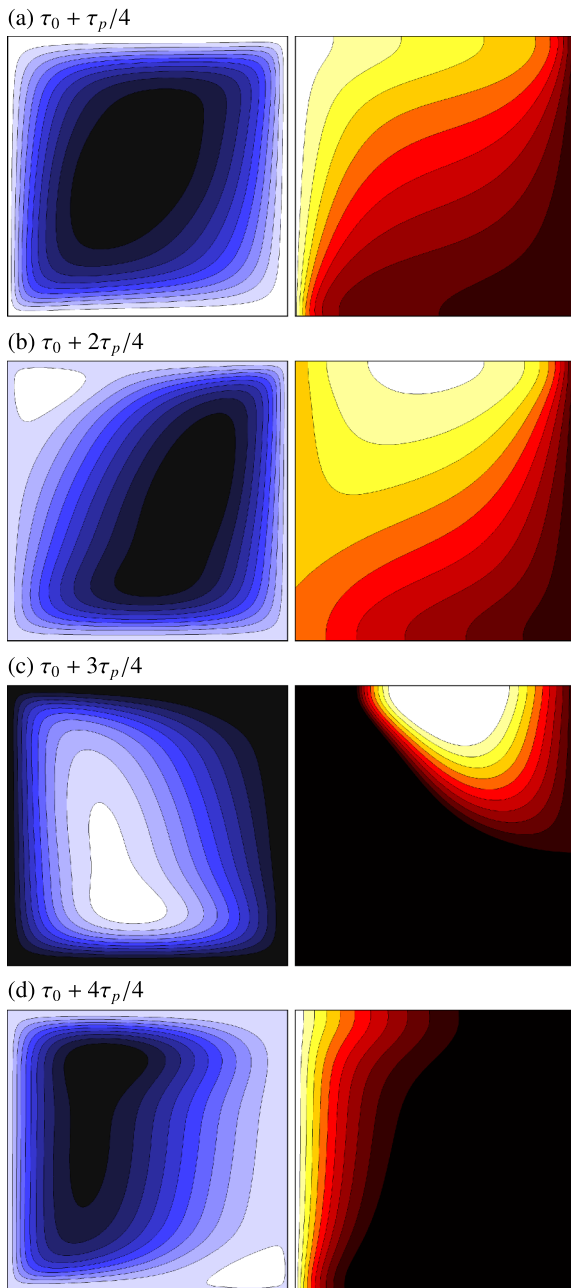


Fig. 4. Contour plots of streamlines (left) and temperature (right) during one period of oscillation for $A = 2$, $f = 2.5$, $\phi = 0.2$, $Ra = 1e6$ and $Ha = 100$. The minimum and maximum levels of ψ and θ , respectively, are (a) 1 to 8, (b) 0.5 to 4.5, (c) 0.5 to 4 and (d) -0.1 to 0.9 , and (a) 0 to 2.8, (b) 0 to 1.5, (c) 0 to 0.1 and (d) 0 to 0.9.

number and the Nusselt number recovers its Hartmann number independence. The Nusselt number curves collapse onto a single curve, which is linear on the log-log scale, demonstrating a power-law dependence on the Rayleigh number with an exponent very close to $1/4$ predicted from theory for the case of natural convection in a cavity without magnetic field and nanoparticles [44]. It can be noted that between the diffusion- and convection-dominated regimes, where the magnetic field suppresses the convection flows, the effect of the Hartmann number on the Nusselt number is significant. From Fig. 5, it can be noted that there is a critical Rayleigh number at which the average Nusselt number attains its minimum. The critical Rayleigh number values obtained at different Hartmann numbers for $\phi = 0.2$ are given in Table 5. Critical Rayleigh number exhibits a power-law relationship

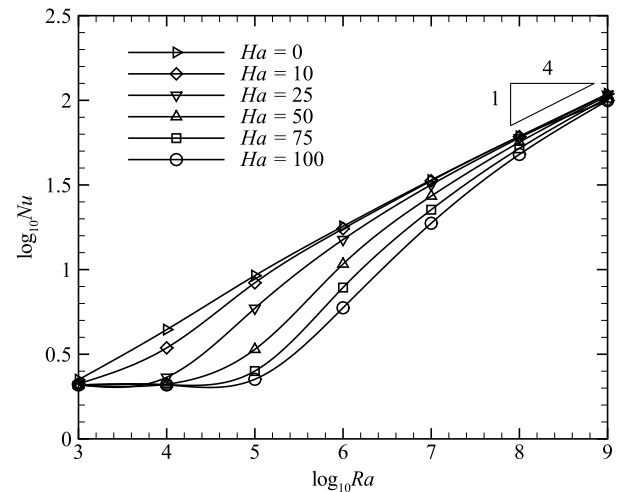


Fig. 5. A plot of $\log_{10}Nu$ against $\log_{10}Ra$ for $A = 2$ and $\phi = 0.2$ at different Hartmann numbers as indicated. Splines are fitted to the data for guidance. A gradient of $1/4$ is provided for comparison with theory.

scaling as $Ra_{crit} \sim Ha^{2.06}$ with a correlation coefficient $r^2 = 0.9683$ when $\log_{10}Ra_{crit}$ is plotted against $\log_{10}Ha$. This follows the prefactors to the buoyancy and Lorentz friction terms in eq. 18, the ratio of which is approximately Ra/Ha^2 , and the balance between which dictates the threshold between the dominance of natural convection and Lorentz force.

Fig. 6 portrays the effect of Hartmann number on the vertical component of velocity (left) and the temperature (right) which are extracted along the horizontal mid-span of the enclosure at different Rayleigh numbers for $A = 2$ and $\phi = 0.2$. It can be noted that the vertical velocity component increases with increasing Rayleigh number and decreases with increasing Hartmann number. This is due to the fact that as Rayleigh increases, a strong buoyant flow occurs within the enclosure which are suppressed at higher Hartmann number. For low and high Rayleigh numbers, where the flow is mainly dominated by conduction and convection, respectively, it is observed that the effect of the Hartmann number on the temperature profiles is insignificant. However, for the intermediate range of Rayleigh number, where the convective flow field is not very strong, the effect of the magnetic field on both the velocity and temperature profiles is significant.

Figs. 7 and 8 plot the temperature and streamfunction for $Ha = 25$ and 100 , respectively, at different Rayleigh numbers. The contours are plotted over the duration of one period of oscillation for $A = 2$ and $\phi = 0.2$. Despite the considerably different Hartmann numbers, the Rayleigh number range is sufficient to get different flow regimes. It can be noted that for $Ha = 25$, the flow passes from a diffusion-dominated regime to a convective-dominated regime prior to $Ra \approx 10^5$. However, for $Ha = 100$, the flow remains in diffusion-dominated regime until $Ra \approx 10^5$, and approaches a convective-dominated regime beyond $Ra = 10^8$. Throughout both figures, the diffusion regime presents temperature fields that exhibit a smooth and gradual variation through the enclosure. No thermal boundary layer is visible on the hot wall and

Table 5
Critical Rayleigh number for the departure from the conduction regime at different Hartmann numbers for the solid fraction $\phi = 0.2$.

Ha	$\log_{10}Ra_{crit}$	Ra_{crit}
10	2.26542	1.84×10^2
25	3.28501	1.93×10^3
50	3.50429	3.19×10^3
75	4.15381	1.42×10^4
100	4.41286	2.59×10^4

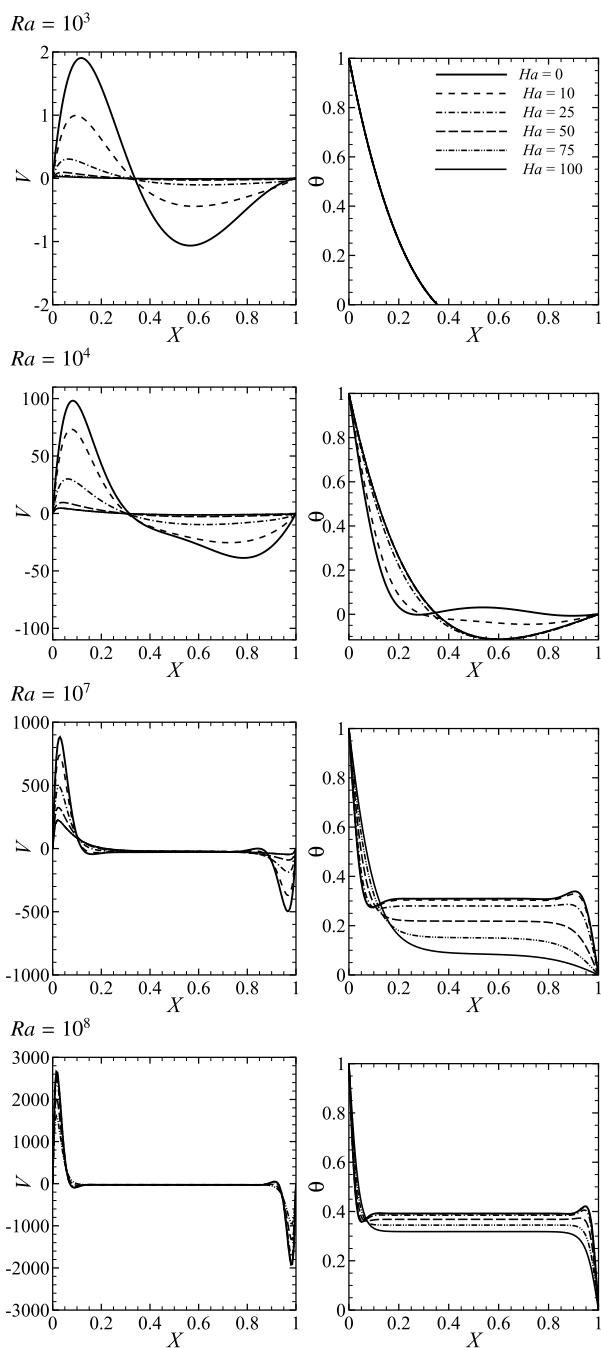


Fig. 6. Plot showing x-variation of vertical velocity component and temperature at $y = 0.5$ at different Rayleigh and Hartmann numbers for $A = 2$ and $\phi = 0.2$.

the isotherms are nearly vertical. The convective regime presents a thin thermal boundary layer next to the hot wall where temperature changes rapidly in the vertical direction, and a region of constant temperature fluid (Ref. 10(c)) extending from the boundary layer to the top wall of the cavity. For the diffusion-convection regime, the isotherms slanted a way from the hot wall and become nearly horizontal at the centre of the cavity at higher Hartmann number.

Fig. 9 shows the variation of the time-average Nusselt number with the solid volume fraction at different Hartmann number for $A = 2$ and $Ra = 10^6$. The results show that as Hartmann number increases from $Ha = 0$ to $Ha = 50$, the time-average Nusselt number along the heated wall increases linearly with increasing solid volume fraction. The increase is more pronounced at $Ha < 50$. However, the variation of the

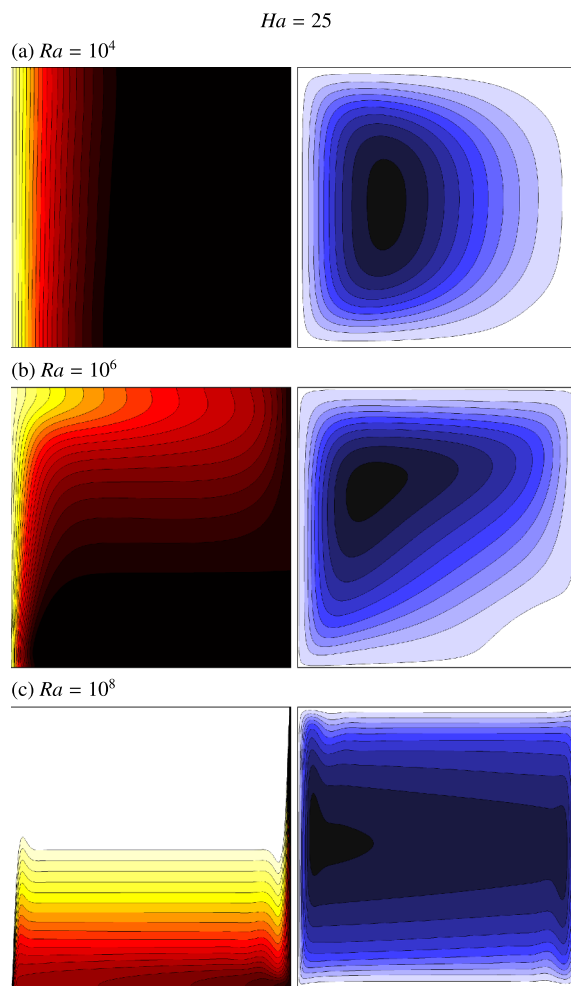


Fig. 7. Contour plots of temperature (left) and streamlines (right) during one period of oscillation. Each case is depicted at the frequency producing maximum heat transfer for $A = 2$, $\phi = 0.2$ and $Ha = 25$ at different Rayleigh number as indicated. Streamline fields: light and dark contours show high and low velocity, respectively. Temperature fields: dark and light contours show cold and hot fluid, respectively.

time-average Nusselt with the solid volume fraction remains nearly constant at $Ha = 75$ and decreases slightly as Hartmann number is increased to $Ha = 100$. This behaviour is due to the effect of magnetic field in the suppression of the buoyant flows of the nanofluids at higher densities of the nanoparticles. In addition, there is a significant change in the slope of the curves as Hartmann number initially increases from $Ha = 10$ to 100 , decreasing by almost 100%.

For a given Hartmann number, the rate of decrease in the time-average Nusselt number with the solid volume fraction is more pronounced at high Ha . For example, the time-averaged Nusselt numbers are almost unchanged for $Ha = 10$, whereas for $Ha = 50$ the value of Nusselt number for the base fluid (i.e. $\phi = 0$) lowered by 40% as more nanoparticles with $\phi = 0.2$ are introduced. However, For $Ha > 50$, the time-average Nusselt number initially decreases as the solid volume fraction increases.

5. Conclusions

Natural convection of an oscillating wall temperature on the left wall of an enclosure filled with a nanofluid and is influenced by a magnetic field has been numerically investigated. The effects of various pertinent parameters such as oscillation amplitudes and forcing frequencies, Hartmann number, Rayleigh number and solid volume

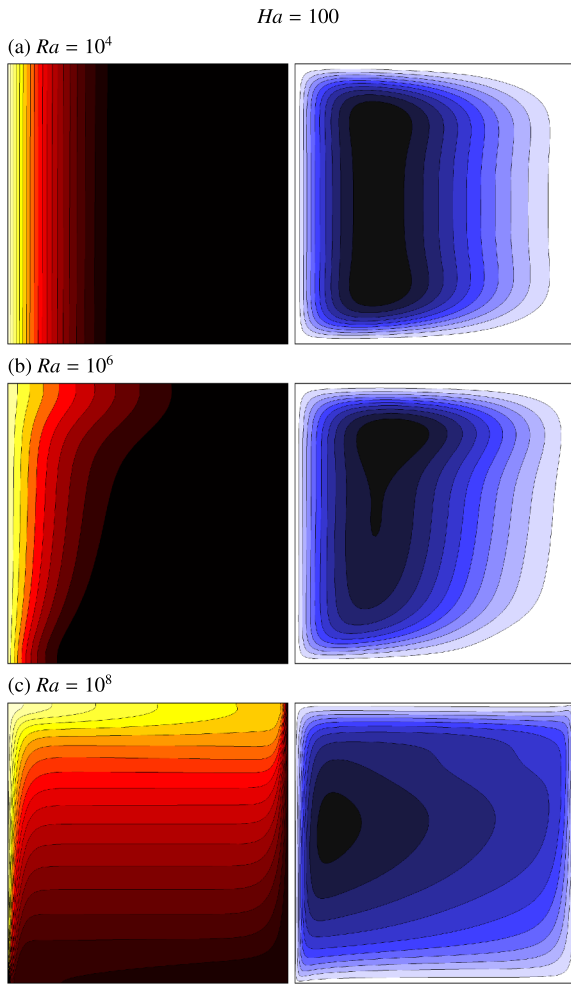


Fig. 8. Contour plots of temperature (left) and streamlines (right) during one period of oscillation. Each case is depicted at the frequency producing maximum heat transfer for $A = 2$, $\phi = 0.2$ and $Ha = 100$ at different Rayleigh number as indicated. Streamline fields: light and dark contours show high and low velocity, respectively. Temperature fields: dark and light contours show cold and hot fluid, respectively.

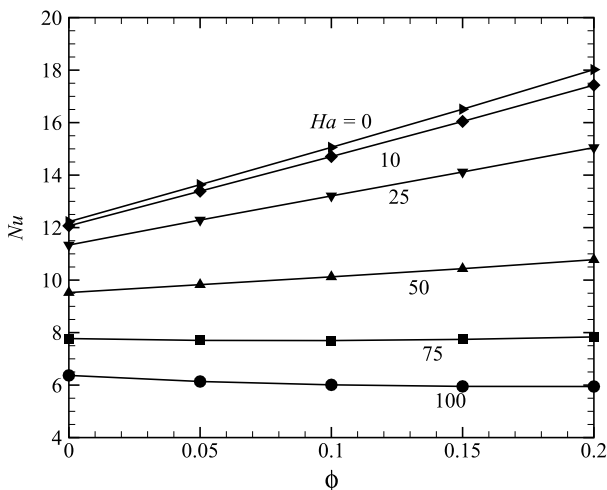


Fig. 9. Variation of time-average Nusselt number with ϕ for $Ra = 10^6$, $A = 2$ and $f = 2.5$ at different Hartmann numbers as indicated. The slopes of $\partial Nu / \partial \phi$ at $Ha = 0, 10, 25, 50, 75$, and 100 are $28.928, 26.756, 6.2272, 0.321$, and -2.0626 , respectively.

fraction on the flow and heat transfer characteristics have been examined for the Prandtl number $Pr = 6.2$.

It is found that there is a substantial enhancement in heat transfer for higher amplitudes where an increase with the peak Nusselt number is observed with increasing the forcing amplitude of the hot wall. As the oscillation amplitude increases, the frequency where the peak Nusselt number occurs, remains almost constant at $f = 2.5$ for $A > 0.5$, and increases to $f = 5$ for $A \leq 0.5$. The flow structure for the frequency at which the peak Nusselt number occurred was characterised by a clockwise rotating primary cells located at centre of the enclosure which fluctuated in intensity for both amplitudes and in the location for the higher amplitude. In addition, a weaker secondary cell was observed at the upper left and right corners of the enclosure at the higher amplitude.

At low Rayleigh number, where the flow is diffusion dominated, the Nusselt number demonstrates Rayleigh number and Hartmann number independence. Above some critical Rayleigh number, the Nusselt number collapses to single curves independent of Hartmann number, and in agreement with theory, i.e. $Nu \propto Ra^{1/4}$.

A strong flow circulation and intense isotherm were observed near the oscillating vertical wall at higher Rayleigh numbers and lower Hartmann numbers for a fixed solid volume fraction of $\phi = 0.2$. The y-velocity and temperature distributions along the horizontal mid-span of the enclosure demonstrate stronger flow fields in the enclosure and higher temperature gradient near the vertical oscillatory hot wall at higher Rayleigh numbers and lower Hartmann numbers. Furthermore, the rate of decrease in the Nusselt number with the solid volume fraction is more pronounced at high Ha .

The effect of the solid volume fraction on the response of the heat transfer inside the cavity strongly depends on the value the Rayleigh number and the Hartmann number. It was found that as Hartmann number increases from $Ha = 0$ to $Ha = 50$, the Nusselt number increases linearly with increasing solid volume fraction. The increase is more pronounced at $Ha < 50$. However, the variation of the Nusselt with the solid volume fraction remains steady at $Ha = 75$ and decreases slightly as Hartmann number is increased to $Ha = 100$. Furthermore, the rate of decrease in the Nusselt number with the solid volume fraction is more pronounced at high Ha .

Acknowledgments

G.J.S. is supported by the Australian Research Council through Discovery Grants DP150102920 and DP180102647, and a National Computational Infrastructure (NCI) high-performance compute time grant under the National Computational Merit Allocation Scheme (NCMAS). NCI is supported by the Australian Government. W.K. Hussam is supported by the Research Council of Australian College of Kuwait, Kuwait through Grant No. IRC-2017-18-PR11.

References

- [1] A. Bejan, C.L. Tien, Laminar natural convection heat transfer in a horizontal cavity with different end temperatures, *J. Thermophys. Heat Transf.* 100 (1978) 641–647.
- [2] G.D.V. Davis, Natural convection of air in a square cavity: a bench mark numerical solution, *Int. J. Numer. Meth. Fl.* 3 (1983) 249–264.
- [3] R.J. Krane, Some detailed field measurements for a natural convection flow in a vertical square enclosure, *Proceedings of the First ASME-JSME Thermal Engineering Joint Conference*, vol. 1, 1983, pp. 323–329.
- [4] K.L. Guo, S.T. Wu, Numerical study of flow and temperature stratifications in a liquid thermal storage tank, *J. Sol. Energy Eng.* 107 (1985) 15–20.
- [5] J.D. Hall, A. Bejan, J.B. Chaddock, Transient natural convection in a rectangular enclosure with one heated side wall, *Int. J. Heat Fluid Flow* 9 (4) (1988) 396–404.
- [6] J. Patterson, S.W. Armfield, Transient features of natural convection in a cavity, *J. Fluid Mech.* 219 (1990) 469–497.
- [7] R.A. Kuyper, T.H.V.D. Meer, C.J. Hoogendoorn, R.A.W.M. Henkes, Numerical study of laminar and turbulent natural convection in an inclined square cavity, *Int. J. Heat Mass Transf.* 36 (11) (1993) 2899–2911.
- [8] M.R. Ravi, R.A.W.M. Henkes, C.J. Hoogendoorn, On the high-rayleighnumber structure of steady laminar natural-convection flow in a square enclosure, *J. Fluid Mech.* 262 (1994) 325–351.

- [9] G. Barakos, E. Mitsoulis, Assimacopoulos DO. Natural convection flow in a square cavity revisited: laminar and turbulent models with wall functions, *Int. J. Numer. Meth. Fl.* 18 (7) (1994) 695–719.
- [10] R.J.A. Janssen, R.A.W.W. Henkes, Influence of prandtl number on instability mechanisms and transition in a differentially heated square cavity, *J. Fluid Mech.* 290 (1995) 319–344.
- [11] N.M. Al-Najem, K.M. Khanafer, M.M. El-Refaei, Numerical study of laminar natural convection in tilted enclosure with transverse magnetic field, *Int. J. Numer. Meth. Heat Fl. Flow* 8 (1998) 651–672.
- [12] A.J. Chamkha, Hydromagnetic combined convection flow in a vertical lid-driven cavity with internal heat generation or absorption, *Numer. Heat Transf. A Appl.* 41 (2002) 529–546.
- [13] T. Grosan, C. Revnic, I. Pop, D.B. Ingham, Magnetic field and internal heat generation effects on the free convection in a rectangular cavity filled with a porous medium, *Int. J. Heat Mass Transf.* 52 (2009) 1525–1533.
- [14] M. Kaneda, T. Tagawa, H. Ozoe, Natural convection of liquid metal under a uniform magnetic field with an electric current supplied from outside, *Exptl. Thermal. Fl. Sci.* 30 (2006) 243–252.
- [15] M. Sathiyamoorthy, A.J. Chamkha, Effect of magnetic field on natural convection flow in a liquid gallium filled square cavity for linearly heated side wall(s), *Int. J. Thermal Sci.* 49 (2010) 1856–1865.
- [16] G.M. Oreper, J. Szekeley, The effect of an externally imposed magnetic field on buoyancy driven flow in a rectangular cavity, *J. Cryst. Growth* 64 (1983) 505–515.
- [17] S. Alchaar, P. Vasseur, E. Bilgen, Natural convection heat transfer in a rectangular enclosure with a transverse magnetic field, *J. Thermophys. Heat Transf.* 117 (1995) 668–673.
- [18] K.M. Khanafer, A.J. Chamkha, Hydromagnetic natural convection from an inclined porous square enclosure with heat generation, *Numer. Heat Transf. A Appl.* 33 (1998) 891–910.
- [19] M. Ashouri, M. Behshad Shafii, Kokande H. Rajabi, MHD natural convection flow in cavities filled with square solid blocks, *Int. J. Numer. Meth. Heat Fl. Flow* 24 (2014) 1813–1830.
- [20] K.M. Khanafer, K. Vafai, M. Lightstone, Buoyancy-driven heat transfer enhancement in a two-dimensional enclosure utilizing nanofluids, *Int. J. Heat Mass Transf.* 46 (19) (2003) 3639–3653.
- [21] A.R. Khaled, K. Vafai, Heat transfer enhancement through control of thermal dispersion effects, *Int. J. Heat Mass Transf.* 48 (2005) 2172–2185.
- [22] K.M. Khanafer, K. Vafai, A critical synthesis of thermophysical characteristics of nanofluids, *Int. J. Heat Mass Transf.* 54 (2011) 4410–4428.
- [23] A.A.K. Vafai, A.R. Khaled, Comparative study between parallel and counter flow configurations between air and falling film desiccant in the presence of nanoparticle suspensions, *Int. J. Energy Res.* 27 (2003) 725–745.
- [24] M. Shafahi, V. Bianco, K. Vafai, O. Manca, Thermal performance of flatshaped heat pipes using nanofluids, *Int. J. Heat Mass Transf.* 53 (2010) 1438–1445.
- [25] M. Shafahi, V. Bianco, K. Vafai, O. Manca, An investigation of the thermal performance of cylindrical heat pipes using nanofluids, *Int. J. Heat Mass Transf.* 53 (2010) 376–383.
- [26] J.A. Eastman, S. Choi, S. Li, W. Yu, L.J. Thompson, Anomalous increased effective thermal conductivities of ethylene glycol-based nanofluids containing copper nanoparticles, *Appl. Phys. Lett.* 78 (2001) 718–720.
- [27] S.P. Jang, S.U. Choi, Role of brownian motion in the enhanced thermal conductivity of nanofluids, *Appl. Phys. Lett.* 84 (2004) 4316–4318.
- [28] S.K. Das, N. Putra, W. Roetzel, Pool boiling characteristics of nano-fluids, *Int. J. Heat Mass Transf.* 46 (2003) 851–862.
- [29] B.X. Wang, L.P. Zhou, X.F. Peng, A fractal model for predicting the effective thermal conductivity of liquid with suspension of nanoparticles, *Int. J. Heat Mass Transf.* 46 (2003) 2665–2672.
- [30] M. Sheikholeslami, M. Gorji-Bandpy, D.D. Ganji, S. Soleimani, Natural convection heat transfer in a cavity with sinusoidal wall filled with Cu–water nanofluid in presence of magnetic field, *J. Taiwan Inst. Chem. E* 45 (2014) 40–49.
- [31] I. Mejri, A. Mahmoudi, M.A. Abbassi, A. Omri, MHD natural convection in a nanofluid-filled enclosure with non-uniform heating on both side walls, *Fluid Dyn. Material Proc.* 10 (2014) 83–114.
- [32] H. Nemati, M. Farhadi, K. Sedighi, H.R. Ashorynejad, E. Fattahi, Magnetic field effects on natural convection flow of nanofluid in a rectangular cavity using the lattice boltzmann model, *SCI IRAN* 19 (2012) 303–310.
- [33] M. Kazmierczak, Z. Chinoda, Buoyancy-driven flow in an enclosure with time periodic boundary conditions, *Int. J. Heat Mass Transf.* 35 (1992) 1507–1518.
- [34] G. Wang, X. Meng, M. Zeng, H. Ozoe, Q.W. Wang, Natural convection heat transfer of copper–water nanofluid in a square cavity with time-periodic boundary temperature, *Heat Transfer Eng.* 35 (2014) 630–640.
- [35] G.J. Sheard, M.P. King, Horizontal convection: effect of aspect ratio on rayleigh number scaling and stability, *Appl. Math. Model.* 35 (4) (2011) 1647–1655.
- [36] W.K. Hussam, T.K. Tsai, G.J. Sheard, The effect of rotation on radial horizontal convection and nusselt number scaling in a cylindrical container, *Int. J. Heat Mass Transf.* 77 (2014) 46–59.
- [37] M. Pirmohammadi, M. Ghassemi, G.A. Sheikhzadeh, The effect of a magnetic field on buoyancy-driven convection in differentially heated square cavity, vol. 45, (2009), pp. 407–411.
- [38] Y. Xuan, W. Roetzel, Conceptions for heat transfer correlation of nanofluids, *Int. J. Heat Mass Transf.* 43 (2000) 3701–3707.
- [39] H.C. Brinkman, The viscosity of concentrated suspensions and solutions, *J. Chem. Phys.* 20 (1952) 571.
- [40] W. Yu, S. Choi, The role of interfacial layers in the enhanced thermal conductivity of nanofluids: a renovated Maxwell model, *J. Nanopart. Res.* 5 (2003) 167–171.
- [41] G.E. Karniadakis, M. Israeli, S.A. Orszag, High-order splitting methods for the incompressible Navier–Stokes equations, *J. Chem. Phys.* 97 (2) (1991) 414–443.
- [42] Y.E. Hammami, M.E. Hattab, R. Mir, T. Mediouni, Numerical study of natural convection of nanofluid in a square enclosure in the presence of the magnetic field, *Int. J. Eng. Adv. Technol.* 4 (2015) 630–640.
- [43] W.K. Hussam, M.C. Thompson, G.J. Sheard, Enhancing heat transfer in a high Hartmann number magnetohydrodynamic channel flow via torsional oscillation of a cylindrical obstacle, *Phys. Fluids* 24 (11) (2012) 113601.
- [44] J. Patterson, J. Imberger, Unsteady natural convection in a rectangular cavity, *J. Fluid Mech.* 100 (1980) 65–86.